THE ASTROPHYSICAL JOURNAL, 590:256–270, 2003 June 10

THE CEPHEID DISTANCE TO NGC 5236 (M83) WITH THE ESO VERY LARGE TELESCOPE[1]

FRANK THIM[2] AND G. A. TAMMANN
Astronomisches Institut der Universität Basel, Venusstrasse 7, CH-4102 Binningen, Switzerland

A. SAHA AND A. DOLPHIN
National Optical Astronomy Observatory, 950 North Cherry Avenue, Tucson, AZ 85726

ALLAN SANDAGE
Observatories of the Carnegie Institution of Washington, 813 Santa Barbara Street, Pasadena, CA 91101

E. TOLSTOY
Kapteyn Instituut, Rijksuniversiteit Groningen, NL-9700AV Groningen, Netherlands

AND

LUKAS LABHARDT
Astronomisches Institut der Universität Basel, Venusstrasse 7, CH-4102 Binningen, Switzerland
Received 2002 December 13; accepted 2003 February 18

ABSTRACT

Cepheids have been observed in NGC 5236 (M83) using the Antu (Unit Telescope 1) 8.2 m telescope of the ESO Very Large Telescope with the Focal Reducer/Low Dispersion Spectrograph 1. Repeated imaging observations have been made between 2000 January and 2001 July. Images were obtained in 34 epochs in the V band and in six epochs in the I band. The photometry was made with the ROMAFOT reduction package and checked independently with DoPHOT and a modified version of HSTPHOT. Twelve Cepheid candidates have periods ranging between 12 and 55 days. The dereddened distance modulus is adopted to be $(m-M)^0 = 28.25 \pm 0.15$, which corresponds to a distance of 4.5 ± 0.3 Mpc. The Cepheid distance of NGC 5253 has been rediscussed and strengthened by its SN 1972E. The mean distance of $(m-M)^0 = 28.01 \pm 0.15$ (based on SN 1972E) shows the galaxy to be a close neighbor of M83, suggesting that the two galaxies may have interacted in the past and thus possibly explaining the amorphous morphology of NGC 5253. The distance difference between M83 and NGC 5253 is only 0.5 ± 0.4 Mpc. The *projected* distance is only ~ 0.15 Mpc. M83 is the principal member of the nearby M83 group containing also, besides NGC 5253, several dwarf members, for five of which tip of the red giant branch distances are available. The adopted group distance of $(m-M)^0 = 28.28 \pm 0.10$ (4.5 ± 0.2 Mpc), together with its mean recession velocity of $v_{\rm LG} = 249 \pm 42$ km s^{-1}, shows again the extreme quietness of the local (1–10 Mpc) expansion field. M83 fits onto the local mean Hubble flow line of the velocity-distance relation (with $H_0 \sim 60$) with no significant deviation, supporting the earlier conclusion that the local velocity expansion field is remarkably cold on a scale of 10 Mpc, contrary to the predictions of the simplest cold dark matter model for large-scale structure. The role of a cosmological constant has been invoked as a possible solution in providing a nearly uniform force field everywhere in the presence of a lumpy galaxy distribution.

Subject headings: Cepheids — distance scale — galaxies: distances and redshifts — galaxies: individual (M83, NGC 5253)

On-line material: FITS file

1. INTRODUCTION

Galaxy distances are the basis of much of extragalactic astronomy and a central theme in cosmology. There is a wide yet poorly tested consensus that the most reliable extragalactic distances come from the period-luminosity (P-L) relation of Cepheid variable stars. If observed in two passbands (V, I), their absorption-corrected distances can be determined. The zero point of the P-L relation is usually based on an adopted distance of the LMC, whose distance is secure to ± 0.1 from a number of distance indicators (see compilations by Federspiel, Tammann, & Sandage 1998; Gibson 2000; Tammann, Sandage, & Reindl 2003b).

The spiral galaxy M83 (NGC 5236; $\alpha = 13^{\rm h}37^{\rm m}01^{\rm s}$, $\delta = -29^\circ 51' 59''$ [J2000.0]), classified as SBc(s) II in the Revised Shapley-Ames Catalog (Sandage & Tammann 1987), is the principal member of a small galaxy group comprising in addition nine probable dwarf members (Karachentsev et al. 2002a). NGC 5253 is an almost certain member of the group. The group is, however, distinct from the NGC 5128 (Cen A) group, which has in addition to NGC 4945 probable dwarf members; this group lies about 12° away from M83 and has a smaller mean distance and a lower mean redshift, according to Karachentsev et al. (2002a).

The distance of M83 is particularly interesting for two reasons: (1) NGC 5253 lies only ~2° from M83. It is a prototype of the amorphous class (Sandage & Brucato 1979). It has been suggested that amorphous galaxies are the result of gravitational interaction (Krienke & Hodge 1974; Hogg et al. 1998), but in the case of NGC 5253, no interacting partner has yet been proposed. Since the distance of NGC 5253 is well known from its Cepheids and Type Ia supernova (SN Ia) 1972E, a good distance of M83 becomes highly

[1] Based on observations collected with the UT1 of the Very Large Telescope, which is operated by the European Southern Observatory.
[2] Visiting Fellow at NOAO.

desirable for comparison. (2) The distances to local galaxies known at present suggest that the local flow pattern of the Hubble expansion field is unexpectedly quiet (Sandage, Tammann, & Hardy 1972; Sandage 1986; Ekholm et al. 2001; Tammann et al. 2003a; Karachentsev et al. 2002b, 2003). M83 provides a valuable additional local datum with which to map the local velocity field.

From the beginning of the modern mapping of the local expansion field, a principal objective has been to determine the velocity dispersion about the mean Hubble flow. Hubble & Humason (1931, 1934) had early estimated that the velocity dispersion about the linear velocity-distance relation was $\lesssim 200$ km s^{-1}. As the estimates of relative distances became better, the value steadily decreased. By 1972 Sandage et al. (1972) could measure an upper limit of $\sigma(\Delta v) \sim 100$ km s^{-1}. This was reduced to ~ 50 km s^{-1} by Sandage & Tammann (1975) in Paper V of their Hubble Constant Steps series. This low value has been confirmed often thereafter by others (e.g., Sandage 1975, 1986; Tammann & Kraan 1978; Ekholm et al. 2001). Also, the many new Cepheid distances to very local galaxies just outside the Local Group in the programs by Hoessel and Saha and their collaborators and other groups (see Mateo 1998 for extensive references) confirm that $\sigma(\Delta v) < 60$ km s^{-1} for distances up to 7 Mpc beyond the Local Group.

Because this extremely low value contradicts the prediction of the simplest cold dark matter model for the formation of large-scale structure by at least a factor of 5 (see Davis & Peebles 1983; Davis et al. 1985; Ostriker 1993; Governato et al. 1997; Bertschinger 1998), continued measurements of the quietness of the Hubble flow over distance scales within 10 Mpc are crucial. The galaxy group with M83 as a member at a mean distance of ~ 4.5 Mpc (determined here) is of special importance.

2. OBSERVATIONS

2.1. *The Instruments*

Repeated imaging of M83 has been made with the ESO Very Large Telescope (VLT) Unit Telescope 1 (UT1; Antu) at Paranal Observatory in Chile. The instrument used was FORS1 (Focal Reducer/Low Dispersion Spectrograph 1) with a 2048×2048 Tektronix CCD with 24 μm pixels. Two different spatial resolutions can be selected. We used the standard resolution collimator, which delivers a lower resolution but larger field size. This provides a field of view of $6\farcm8 \times 6\farcm8$ and a pixel scale of $0\farcs2$ pixel^{-1}. The large collecting area makes FORS1 superior to the *Hubble Space Telescope* (*HST*) Wide-Field Planetary Camera 2 (WFPC2) for the detection of Cepheids in NGC 5236. For the determination of the internal absorption, observations with Bessel *V*- and *I*-band filters (Szeifert & Böhnhardt 2001) have been made.

2.2. *The Data*

A field northwest of the center of M83 was chosen. Images of the center of M83 would be too crowded for high-quality photometry. A $20' \times 20'$ field of the Digitized Sky Survey (DSS) at the position of M83 is shown in Figure 1. The square box shows the FORS1 $6\farcm8 \times 6\farcm8$ field of view. There are in total 34 epochs in the *V* passband and six epochs in the *I* passband over a period of 1.5 yr, from 2000 January 4 to 2001 July 23. Each individual epoch consists of two to four subexposures having exposure times between 400 and 600 s. A journal of observations is given in Table 1. The seeing is almost always subarcsecond and, for some epochs, exceptionally good ($\leq 0\farcs5$). Such exceptional seeing conditions are required at least in one *V* and one *I* image to get accurate stellar positions, which are used to disentangle the stellar photometry in images of lower seeing quality. The VLT image of the epoch with the best seeing, i.e., V_17, is shown in Figure 2.

3. DATA PROCESSING AND PHOTOMETRY

In order to gain control over the errors introduced by individual photometry procedures and calibrations, the data have been processed independently by us using three different photometry software programs with three independent calibrations: the ROMAFOT package (Buonanno et al. 1983) as implemented in ESO-MIDAS (European Southern Observatory–Munich Image Data Analysis System; ESO 1992), which was developed for crowded fields, DoPHOT (Schechter, Mateo, & Saha 1993) as modified by one of us (A. Saha) for ground-based images, and a modified version of HSTPHOT (Dolphin et al. 2002). ROMAFOT has been used for the photometry of all epochs including the variable search, whereas DoPHOT and HSTPHOT have been used only to process the best *V* and *I* images to compare the calibrations with respect to each other. A detailed discussion of photometry with ROMAFOT, including artificial-star experiments and undersampling, can be found in Thim (2001), and previous applications of ROMAFOT in Saha et al. (2001b), Tammann et al. (2003a), and Thim (2000).

3.1. *Data Reductions*

The FORS1 direct-imaging observations were performed in service mode by Paranal Science Operations staff. We used the pipeline-reduced images that were provided by the Garching Quality Control group, which were bias-subtracted and flat-fielded for us. The raw images have been reduced independently and checked with the pipeline-produced images. No significant differences were found. A point to note is the gain setting. FORS1 has different gain settings. First, the gain is different for the four different quadrants (four-port readout). Second, the gain setting is different for the science images and for the standard-star observations. The science images are always taken with low gain; the standard-star observations are taken with either low or high gain. While the relative gain between the four quadrants is pipeline-calibrated, the overall gain settings between science and standard-star images have to be corrected individually.

3.2. *Relative Photometry with ROMAFOT*

The two best images, V_17 and I_04, taken with a seeing of $\leq 0\farcs50$, were used as reference images. Attempts to create an even deeper reference image by co-adding the images of various epochs were unsuccessful because of variable seeing and nonnegligible field shifts and field rotation.

Twenty-five isolated, unsaturated stars were selected on V_17 and I_04 to establish the mean point-spread functions (PSFs) in *V* and *I*. The PSF of each image was found not to vary significantly with position.

Stars on V_17 and I_04 brighter than a certain limit were then fitted with the appropriate PSF and subtracted from

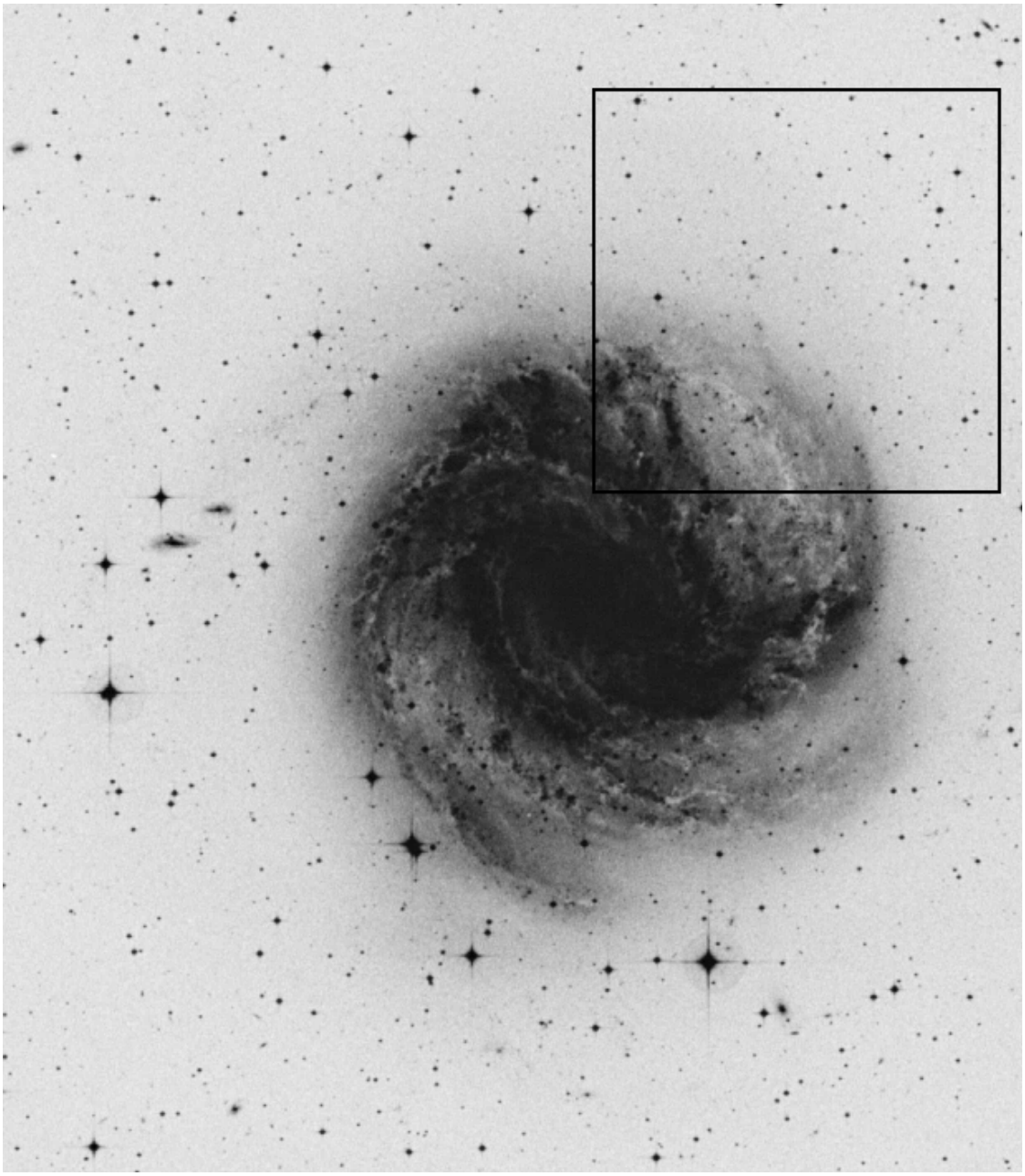

FIG. 1.—DSS image of the $20' \times 20'$ field centered at the position of M83. North is up and east is to the left. The insert shows the $6.'8 \times 6.'8$ FORS1 field of view northwest of the center of M83.

the field. The procedure was repeated on the residual images in an iterative process, cutting at fainter and fainter limits.

The resulting list of stars (separately in V and I) and their positions were used as a master list for all other images. The master positions were transformed into positions on the individual images by means of a matching algorithm.

All stars of the master lists were searched for on the images in V and I, respectively, and fitted with the mean PSF of that image going stepwise, as above, to the faintest possible stars. The mean PSF was determined using the same 25 stars, if possible, as above.

3.3. *Standardizing the Photometry*

The PSF-fitted magnitudes were corrected for atmospheric extinction. Since the Landolt standard stars (see below) were observed at almost constant air mass, it was not possible to determine nightly extinction coefficients. Mean extinction coefficients from the VLT World Wide Web site have therefore been adopted.

The corrected PSF magnitudes of all V and I images are still on arbitrary zero points because of different exposure times and seeing. The mean zero-point shifts of each image with respect to the template images V_17 and I_04, respectively, were determined using all well-fitted stars and then subtracted. Thus, all PSF magnitudes are converted to the same zero point.

The next step is to convert the PSF magnitudes, which rely on the core of the PSF, to aperture magnitudes by means of additive aperture corrections (ACs). The AC was determined for the images V_17 and I_04 by performing aperture photometry on all sufficiently isolated, unsaturated

TABLE 1
OBSERVATION LOG

Archival Image ID[a]	HJD[b]	Exposure Time (s)	Filter	Seeing[c]	Air Mass[d]	Image ID[e]
FORS.2000-01-05T08:02–08:20	51548.345	3 × 500	*V*	0.55–0.68	1.34	V_01
FORS.2000-01-09T08:22–08:40	51552.360	3 × 500	*V*	0.61–0.67	1.21	V_02
FORS.2000-01-18T07:48–08:06	51561.336	3 × 500	*V*	0.57–0.67	1.20	V_03
FORS.2000-02-04T08:00–08:18	51578.343	3 × 500	*V*	0.60–0.66	1.04	V_04
FORS.2000-02-04T08:28–09:00	51578.367	4 × 600	*I*	0.56–0.59	1.01	I_01
FORS.2000-02-04T09:12–09:30	51578.394	3 × 500	*V*	0.51–0.55	1.00	V_05
FORS.2000-02-05T09:03–09:21	51579.386	3 × 500	*V*	1.21–1.39	1.00	V_06
FORS.2000-02-08T05:58–06:26	51582.261	4 × 500	*V*	0.58–0.79	1.29	V_07
FORS.2000-03-12T06:06–06:25	51615.262	3 × 500	*V*	0.75–0.88	1.01	V_08
FORS.2000-03-12T06:35–06:53	51615.281	3 × 500	*V*	0.62–0.75	1.00	V_09
FORS.2000-03-12T07:04–07:34	51615.301	3 × 500	*V*	0.57–0.64	1.00	V_10
FORS.2000-03-12T07:33–07:51	51615.320	3 × 500	*V*	0.64–0.73	1.02	V_11
FORS.2000-03-12T08:01–08:19	51615.340	3 × 500	*V*	0.70–0.74	1.04	V_12
FORS.2000-03-12T08:29–08:47	51615.359	3 × 500	*V*	0.81–0.82	1.08	V_13
FORS.2000-03-12T08:57–09:29	51615.383	4 × 600	*I*	0.83–0.94	1.16	I_02
FORS.2000-03-13T03:37–04:06	51616.160	4 × 500	*V*	0.62–0.66	1.31	V_14
FORS.2000-03-13T04:16–04:27	51616.184	2 × 600	*I*	0.69–0.83	1.21	I_03
FORS.2000-03-15T06:33–06:51	51618.281	3 × 500	*V*	1.14–1.75	1.00	V_15
FORS.2000-03-31T06:00–06:19	51634.256	3 × 500	*V*	0.52–0.61	1.01	V_16
FORS.2000-04-05T06:16–06:34	51639.264	3 × 500	*V*	0.35–0.40	1.03	V_17
FORS.2000-05-06T04:54–05:26	51670.210	4 × 500	*V*	0.69–0.93	1.09	V_18[f]
FORS.2000-07-01T01:21–01:36	51726.057	3 × 400	*V*	0.88–1.04	1.09	V_19
FORS.2000-07-07T23:06–23:21	51732.964	3 × 400	*V*	0.51–0.57	1.00	V_20
FORS.2000-07-07T23:29–23:57	51732.983	3 × 600	*I*	0.46–0.49	1.01	I_04
FORS.2000-07-26T00:11–00:26	51751.008	3 × 400	*V*	0.92–1.00	1.16	V_21
FORS.2000-07-30T23:27–23:42	51755.981	3 × 400	*V*	0.95–1.05	1.10	V_22
FORS.2000-08-07T23:37–23:52	51763.985	3 × 400	*V*	1.00–1.14	1.21	V_23
FORS.2001-02-17T07:07–07:23	51957.303	3 × 400	*V*	1.06–1.65	1.04	V_24
FORS.2001-03-22T04:26–04:41	51990.191	3 × 400	*V*	0.54–0.89	1.09	V_25
FORS.2001-03-27T06:39–06:54	51995.280	3 × 400	*V*	0.70–0.75	1.02	V_26
FORS.2001-05-17T00:37–00:52	52046.026	3 × 400	*V*	0.61–0.83	1.11	V_27
FORS.2001-05-20T23:17–23:42	52049.975	4 × 400	*V*	0.64–0.77	1.26	V_28[f]
FORS.2001-05-26T03:17–03:32	52055.135	3 × 400	*V*	1.39–1.58	1.05	V_29
FORS.2001-05-28T02:16–02:31	52057.096	3 × 400	*V*	0.66–0.79	1.01	V_30
FORS.2001-06-16T01:54–02:16	52076.081	3 × 600	*I*	0.47–0.53	1.06	I_05
FORS.2001-06-20T23:47–00:08	52080.995	3 × 600	*I*	0.45–0.56	1.00	I_06
FORS.2001-06-26T23:23–23:38	52086.975	3 × 400	*V*	0.49–0.53	1.00	V_31
FORS.2001-07-17T00:05–00:20	52107.003	3 × 400	*V*	0.48–0.55	1.07	V_32
FORS.2001-07-20T00:25–00:40	52110.019	3 × 400	*V*	0.68–0.83	1.14	V_33
FORS.2001-07-23T23:30–23:45	52113.980	3 × 400	*V*	0.73–1.06	1.06	V_34

[a] The image IDs as used in the archive, i.e., the instrument prefix followed by a time stamp. The time stamp in this table is year, month, date, hour, and minute (UTC). Instead of listing all images, the ranges of the subexposures are shown.
[b] Heliocentric Julian date; 2,400,000.5 at midexposure.
[c] The range of FWHM seeing conditions for all subexposures.
[d] The average air mass.
[e] The name of the combined images. Each combined image consists of two to four subexposures.
[f] Not all subimages have been used to create the combined image; i.e., FORS.2000-05-06T05:12 and FORS.2001-05-20T23:17 have not been used. FORS.2000-05-06T05:12 has been exposed twice; FORS.2001-05-20T23:17 has been taken above the requested image quality and repeated.

stars with flat growth curves. Only four stars in V_17 and five stars in I_04 were accepted for the best mean ACs. The random error of the adopted mean ACs is 0.02 mag in *V* and 0.01 mag in *I*. The value of the AC depends on the selected stars; the systematic error of the AC is estimated using different samples of stars, i.e., the standard deviation of different solutions for the AC. Their systematic error is estimated to be 0.05.

The aperture magnitudes are converted into instrumental magnitudes by adding the appropriate AC to all stars of the various images. The instrumental magnitudes were then transformed into standard magnitudes. The transformation equations were determined from 13 Landolt standard stars, covering the color range $-0.53 < (V-I) < 1.95$ in the fields Ru 152 and PG 0231, which were observed together with V_17 and I_04. The resulting equations are

$$V = V_{\rm instr} + 0.05(\pm 0.012) * (V_{\rm instr} - I_{\rm instr}) + 27.77(\pm 0.007)\ , \quad (1)$$

$$I = I_{\rm instr} - 0.04(\pm 0.013) * (V_{\rm instr} - I_{\rm instr}) + 26.90(\pm 0.011)\ ; \quad (2)$$

$V_{\rm instr}$ and $I_{\rm instr}$ are the instrumental magnitudes, corrected

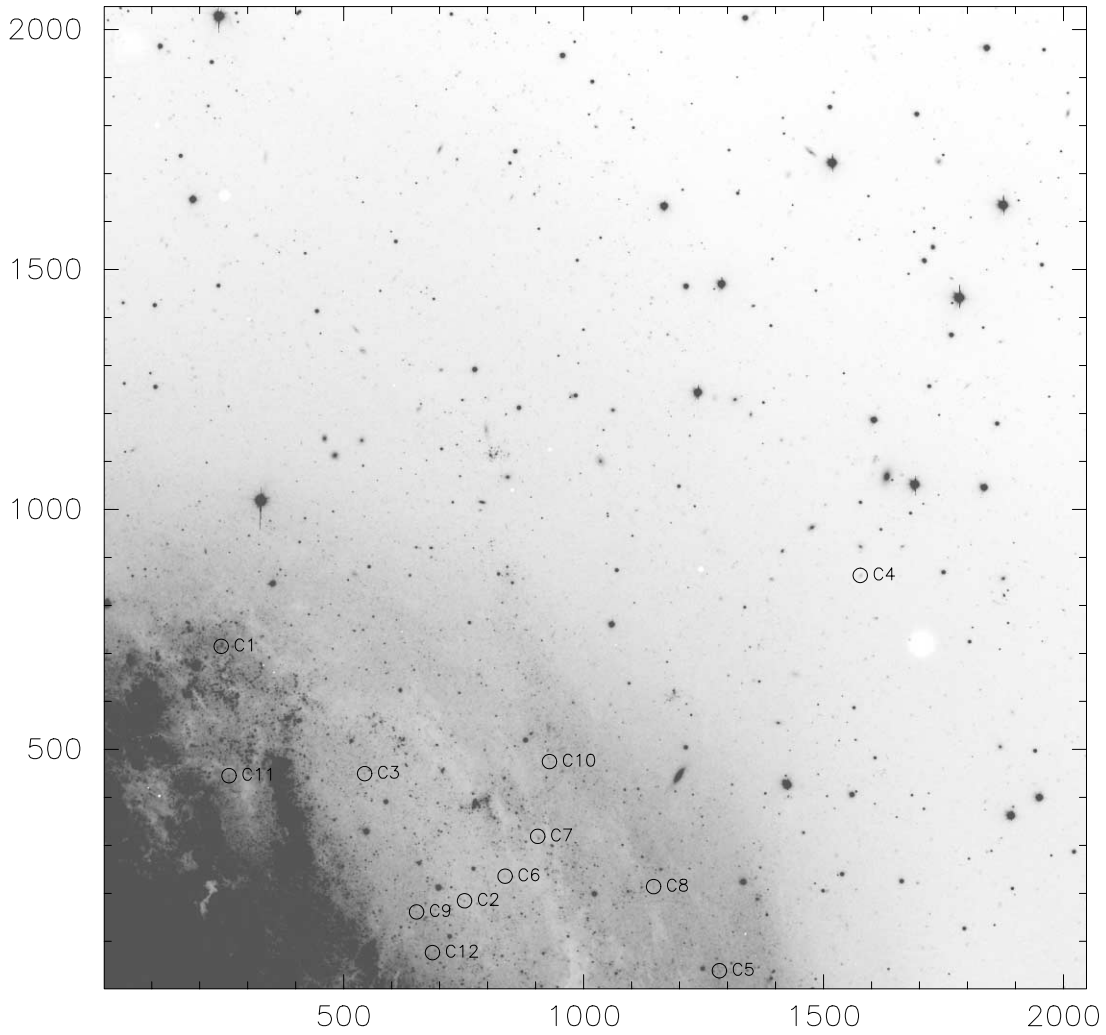

FIG. 2.—VLT FORS1 *V* image of the target field northwest of the center of M83 that illustrates the high spatial resolution. Marked objects are the Cepheids in Table 2. We provide a deep FITS image of the field in the electronic edition of the Journal, which has better quality information than can be printed on paper. The *X* and *Y* position values listed in Table 2 correspond to the FITS image provided.

for extinction. The standard system is reproduced to within ± 0.01 with an rms error of 0.02 mag in *V* and in *I*.

3.4. *Comparing Results from the Different Photometric Calibrations with ROMAFOT, DoPHOT, and HSTPHOT*

The combined *V* and *I* images with the best seeing, i.e., V_17 and I_04, were independently reduced with three different software programs (by three different members of our group).

The ROMAFOT photometry is characterized in detail above. The DoPHOT photometry was carried out as described in Saha, Claver, & Hoessel (2002). The photometry with the modified version of HSTPHOT was carried out as described in Dolphin et al. (2002). A comparison of the resulting magnitudes in *V* and *I* is presented in Figures 3–5. Note that the apparent upturn of the point distributions at the faintest levels is simply due to the respective cutoffs of the different magnitude systems; i.e., it is a bias due to incompleteness.

The AC was determined independently for each photometry by different members of our group with a number of undisturbed stellar images; different stars were used for the three different software packages. The resulting independent photometric zero points agree to within 0.03 in *V* (at $V = 20.0$) and *I* (at $I = 19.0$). We have decided to use the zero points in *V* and *I* of the ROMAFOT system throughout this paper because they lie in between the zero points of DoPHOT and HSTPHOT. The adopted zero points are estimated to be accurate to within ± 0.03 mag.

Fainter than the level of the adopted common zero point, i.e., at $V > 20.0$, $I > 19.0$, the photometric scales of the three independent reduction procedures differ slightly. The three sets of *V* magnitudes of about 250 stars with $V < 23.5$ were compared. They reveal a scale difference between ROMAFOT and DoPHOT of 0.013 ± 0.002 mag mag^{-1} and between ROMAFOT and HSTPHOT of 0.023 ± 0.001 mag mag^{-1}. The corresponding scale difference in *I*, again from about 250 stars with $I < 22.5$, is between ROMAFOT and DoPHOT 0.015 ± 0.002 mag mag^{-1} and between ROMAFOT and HSTPHOT 0.035 ± 0.001 mag mag^{-1}. The sense of the differences is that ROMAFOT is always fainter. We have adopted an intermediate scale. This results in a mean correction of all ROMAFOT magnitudes by 0.009 mag mag^{-1} in *V* and 0.017 mag mag^{-1} in *I*. These

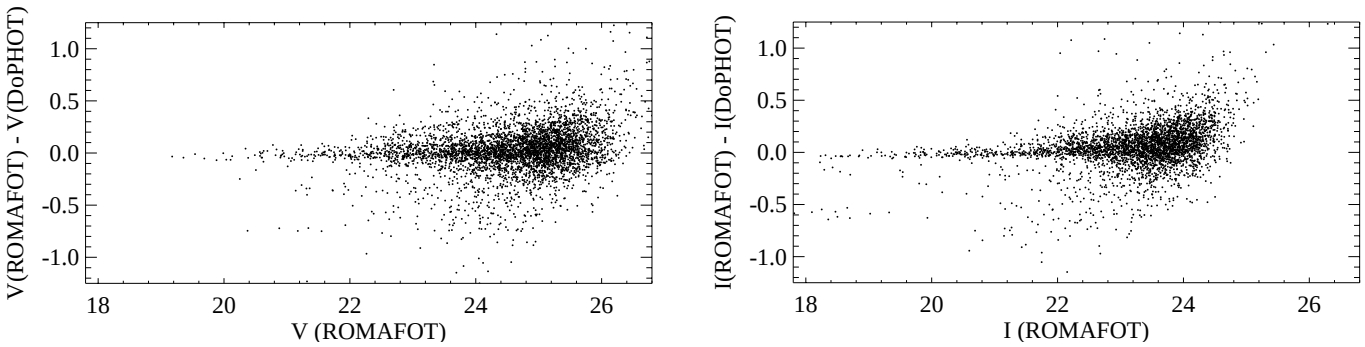

FIG. 3.—Comparison of V (*left*) and I (*right*) magnitudes derived from measurements obtained with ROMAFOT and DoPHOT and a matching radius of 1 pixel.

corrections have been individually applied to all Cepheid magnitudes in Table 2. The maximum corrections of the faintest Cepheid magnitudes amount to -0.04 mag in V and -0.07 mag in I.

Photometry at these levels of faintness and crowding are extremely vulnerable to how the background sky is measured. The three programs have some differences in their respective prescriptions for estimating background. ROMAFOT and DoPHOT fit the background as part of the PSF fitting. HSTPHOT estimates background from the statistics of pixels surrounding the object. There are pros and cons to both approaches, and a philosophical discussion is beyond the scope of this paper. The differences in background that result from such procedural differences are small, but even systematic differences of a few analog to digital units (ADUs; of the order of sampling errors) can produce noticeable differences in the measured magnitudes of faint stars. If program A measures sky systematically lower than program B, the stars measured by A will be brighter than those measured by B. These effects are negligible for brighter stars, but as one approaches the detection limit, the differences increase.

There is another, perhaps more significant way in which background measurements can be different. All three of the programs have a procedure where objects already identified are subtracted before a background estimate is made. However, the procedures by which objects are identified are different, and thus the exact list of objects that are subtracted from a given patch of sky will be different. Again, this results in systematic differences in measured background and manifests as differences in scale for measured magnitudes near the faint end. Because of the nature of luminosity functions, both of stars and of background galaxies, the problem gets more acute as one goes fainter.

In the face of this, there is no clear-cut "correct" prescription. Instead, the differences in resulting magnitudes for the objects of interest that are produced by different competent photometry procedures are a measure of the robustness of the magnitude measurements.

The random error of a single magnitude can be determined from a comparison of the values obtained by the three different reduction procedures after zero-point and scale differences are removed. The rms deviation of the triple measurements of 250 stars with $\langle V \rangle \sim 23.0$ and $\langle I \rangle \sim 22.0$ is 0.05 mag at this level and increases, of course, toward fainter magnitudes.

3.5. *The Color-Magnitude Diagrams*

The observed color-magnitude diagrams (CMDs) obtained with ROMAFOT, DoPHOT, and HSTPHOT photometry are presented in Figures 6–8, respectively.

Stars brighter than $V = 19.2$ and $I = 18.3$ are saturated and have therefore not been included in the object list. The number of well-fitted stars with V *and* I is $\sim$9000 in the case of ROMAFOT, $\sim$38,000 for DoPHOT, and $\sim$20,000 for HSTPHOT. These numbers are not directly comparable because in each case different lower fitting limits have been set, which were guided by a subjective estimate of what is practical and desirable. In addition, the total number of stars in each list can be altered by choosing different parameters like goodness of fit, signal-to-noise ratio, and, in the case of HSTPHOT, also object sharpness.

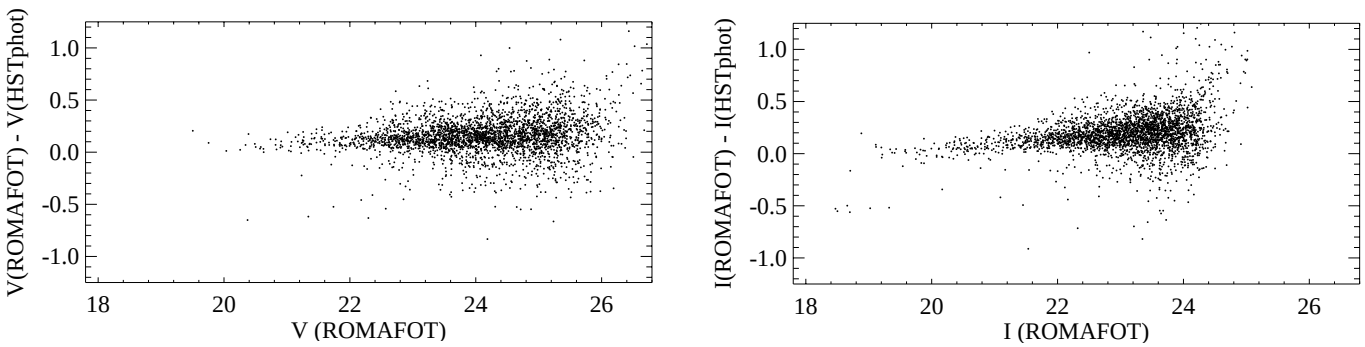

FIG. 4.—Same as Fig. 3, but for magnitudes derived from measurements obtained with ROMAFOT and HSTPHOT

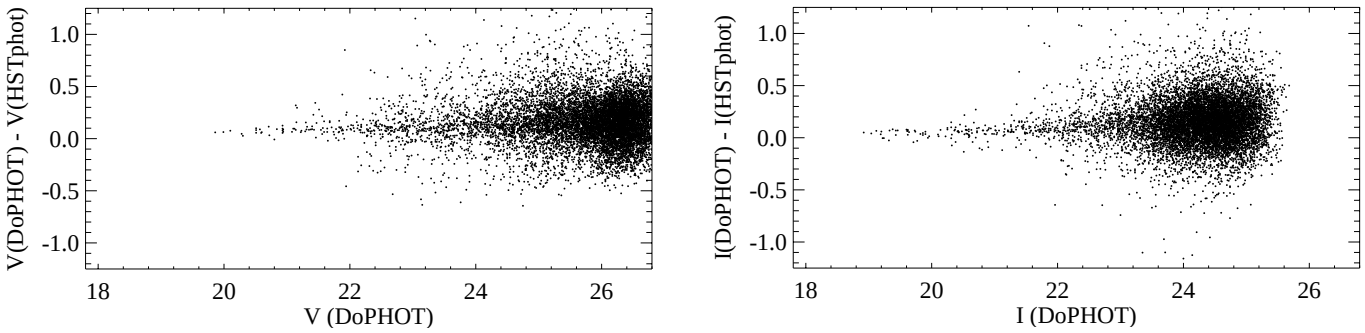

FIG. 5.—Same as Fig. 3, but for magnitudes derived from measurements obtained with DoPHOT and HSTPHOT

At brighter magnitudes, for instance, $V < 24.5$, the number of stars for which V and I magnitudes were obtained with the three different reduction procedures is more comparable: 3666 stars from ROMAFOT stand against 3469 stars from HSTPHOT and 6012 stars from DoPHOT.

The reason for the different number of stars is the different star-searching routines employed. The number of selected stars increases with the decreasing size of the area to define the "sky." DoPHOT and HSTPHOT employed a particularly small number of pixels for the "sky" definition in the star-searching routines. In contrast, ROMAFOT uses a relatively large "sky" in the star-searching routine.

The CMDs of ROMAFOT show a number of blue stars at faint levels that are missing in the other CMDs. This indicates that the ROMAFOT magnitudes have larger scatter below $V \sim 25$.

The comparison with DoPHOT and HSTPHOT show that the ROMAFOT procedure used here is adequate for the discovery of the brightest and hence most reliable Cepheids in M83.

3.6. *Identification of the Variable Stars*

The identification of the variable stars is based on the method by Lafler & Kinman (1965) and is described in Saha & Hoessel (1990). The quantities Θ and the standard deviation $\sigma(V)$ as a function of V over all 34 epochs were used to identify the variable candidates. If P is the period of a supposed variable star, m_i the measured magnitude at the ith epoch, and $\overline{m}$ the average over the n values of m_i, and if the values for m_i are arranged in increasing order of phase, then Θ is defined as

$$\Theta(P) = \frac{\sum_{i=1}^{n}(m_{i+1} - m_i)^2}{\sum_{i=1}^{n}(m_i - \overline{m})^2} \, . \tag{3}$$

A minimum in the spectrum of Θ indicates a possible period.

We have adopted $\Theta_{\min}$, i.e., the lowest smoothed value, obtained by varying the period between 1 and 570 days. Several hundred stars were suspected to be variable on the basis of ROMAFOT photometry. The light curves of these possible candidates with reasonable values of Θ and σ were individually inspected by eye, they were scrutinized, and 12 bona fide Cepheids were retained, of which 10 have also good light curves in I.

The selection criteria of whether a star is a Cepheid or not are subjective. The criteria that have been used here are the quality of the light curve in V, the quality of the light curve in I, the phase coherence between the V and the I light curves, and the shape of the spectrum of Θ. The curves are always smoothed to prevent spikes from indicating spurious periods. A star is more likely to be a Cepheid if the minima of Θ are broad and a second pronounced minimum exists at the two-fold period.

TABLE 2

V AND *I* MAGNITUDES, PERIODS, AND POSITIONS OF THE SELECTED CEPHEIDS

Object ID (1)	$\langle V \rangle$ (2)	$\langle I \rangle$ (3)	Period (days) (4)	X (5)	Y (6)	R.A. (J2000.0) (7)	Decl. (J2000.0) (8)
C1	22.23	21.12	43.52	245.33	715.22	13 36 55.78	−29 48 00.67
C2	22.61	21.59	54.92	752.38	185.02	13 36 47.99	−29 49 46.56
C3	23.52	22.75	28.95	544.20	449.98	13 36 51.18	−29 48 53.62
C4	23.02	22.03	33.16	1577.03	863.07	13 36 35.33	−29 47 31.12
C5	23.35	22.31	28.31	1283.45	39.25	13 36 39.84	−29 50 15.73
C6	24.03	22.57	28.63	836.94	236.24	13 36 46.68	−29 49 36.37
C7	23.22	22.27	32.55	904.89	319.27	13 36 45.65	−29 49 19.80
C8	23.96	23.17	14.17	1146.40	214.52	13 36 41.95	−29 49 40.77
C9	24.05	22.97	12.47	652.41	161.79	13 36 49.54	−29 49 51.15
C10	24.11	23.05	14.21	929.42	475.08	13 36 45.27	−29 48 48.64
C11	23.42	...	26.22	261.55	445.71	13 36 55.52	−29 48 54.40
C12	24.34	...	19.25	685.64	77.02	13 36 49.02	−29 50 08.13

NOTE.—Units of right ascension are hours, minutes, and seconds, and units of declination are degrees, arcminutes, and arcseconds.

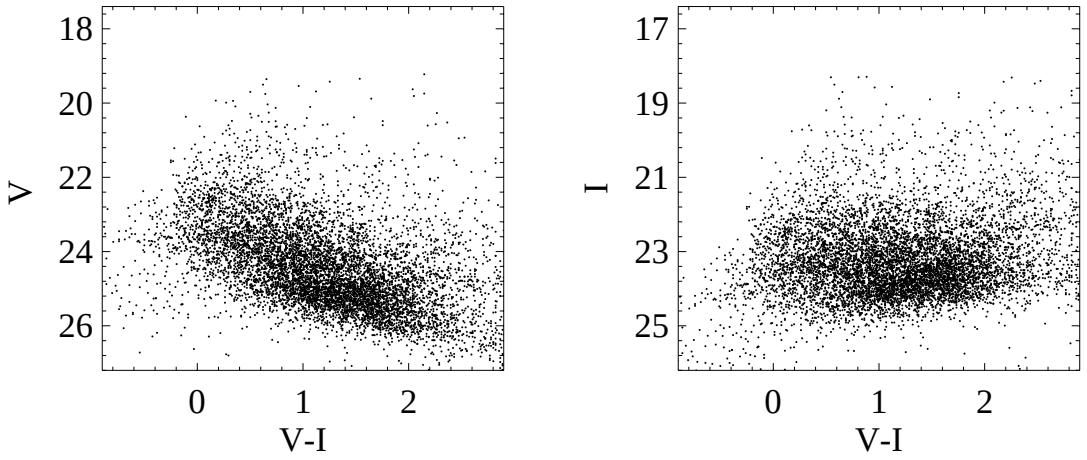

FIG. 6.—$V-I$ vs. V CMD obtained with ROMAFOT

The mean magnitude $\langle V \rangle$, i.e., the magnitude of the phase-weighted intensity average, was calculated for each Cepheid analog to Saha & Hoessel (1990) using

$$\langle V \rangle = -2.5 \log_{10} \sum_{i=1}^{n} 0.5(\Phi_{i+1} - \Phi_{i-1}) 10^{-0.4 m_i} , \quad (4)$$

where n is the number of observations, m_i the magnitude, and Φ_i the phase of the ith observation in order of increasing phase. Intensity-weighted magnitudes can be biased because of missing measurements. The phase-weighted intensity mean gives isolated points more weight than closely spaced ones, which makes it superior to a straight intensity mean.

The method to determine the corresponding mean $\langle I \rangle$ magnitude from the few available epochs in I is described in Labhardt, Sandage, & Tammann (1997). Information on the shape and the amplitude of the complete V light curve as well as the typical phase shift between V and I are used to derive a value of $\langle I \rangle$ from every single I magnitude:

$$\langle I \rangle = I(\phi_V) + [\langle V \rangle - V(\phi_V)] + \Delta V C_{V \to I}(\phi) , \quad (5)$$

where ΔV is the V amplitude, $\langle V \rangle$ the phase-weighted mean V magnitude, ϕ the phase of the light curve, and $C_{V \to I}(\phi)$ the empirical function for the transformation between V and I magnitudes that is tabulated by Labhardt et al. (1997). The mean of the individual $\langle I \rangle$ magnitudes yields the adopted value of $\langle I \rangle$ and its error.

The light curves of the Cepheid candidates are shown in Figure 9. The candidates C11 and C12 have reasonable light curves in V but no counterpart in I. Besides those 12 candidates, no further Cepheid candidates have been accepted. Inspection of images (done before period analysis was performed) indicate that C2, C3, C5, C6, C8, C9, and C10 show no evidence of crowding or blending whatsoever. We cannot rule out this possibility based on this inspection for the other objects.[3] The error bars in Figure 9 as a function of apparent magnitude have been determined from the reproducibility of artificial stars of known magnitude.

The 12 Cepheids are listed in Table 2. Column (1) gives the designation of the Cepheid, column (2) the period, columns (3) and (4) the ROMAFOT mean magnitudes, and columns (5) and (6) its position on the template image V_17. The list of Cepheids with $P > 12$ days has no claim for completeness. The spacing of the observing epochs, mainly dictated by

[3] We provide a deep FITS image of our field in the electronic edition of the Journal. This is better quality information than the image in Fig. 2.

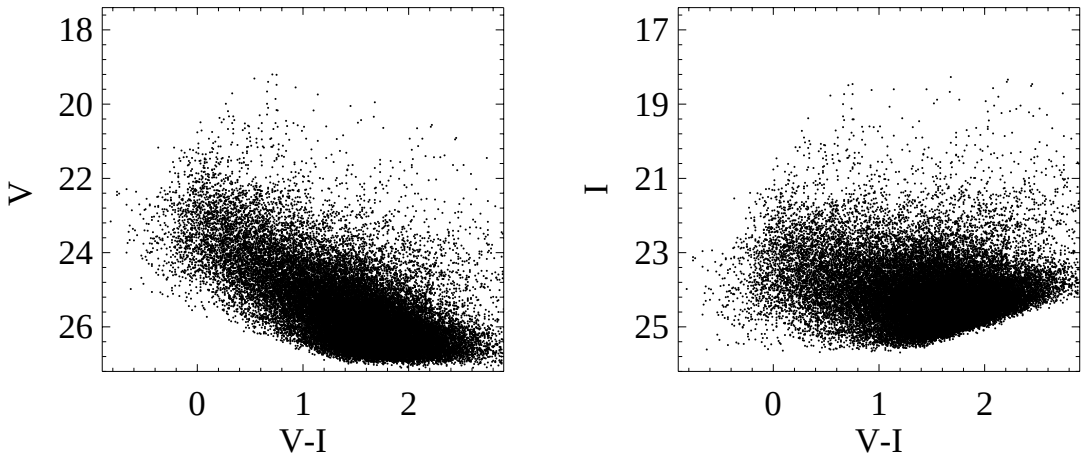

FIG. 7.—$V-I$ vs. V CMD obtained with DoPHOT

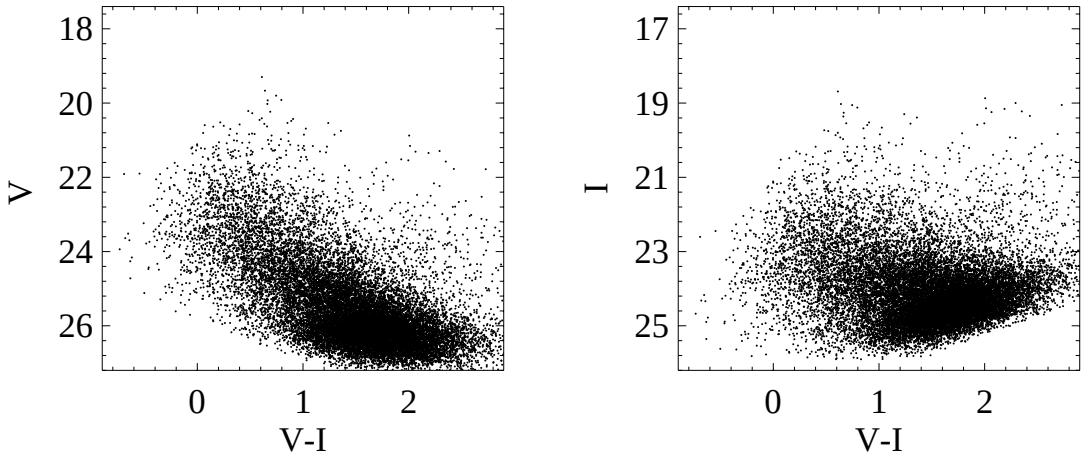

FIG. 8.—$V-I$ vs. V CMD obtained with a modified version of HSTPHOT

seeing and weather conditions, may have made additional Cepheids undetectable within the surveyed field.

4. THE PERIOD-LUMINOSITY RELATION AND THE DISTANCE MODULUS

4.1. *The P-L Relations in V and I*

In a first step we adopt the P-L relation in V and I from Madore & Freedman (1991) as

$$M_V = -2.76 \log P - 1.40 , \quad (6)$$

$$M_I = -3.06 \log P - 1.81 . \quad (7)$$

The zero point of equations (6) and (7) is based on an assumed LMC modulus of 18.50.

The P-L relations in V and I with the slopes of equations (6) and (7) are fitted to the 12 Cepheids with V magnitudes and the 10 Cepheids with I magnitudes in Figure 10. Comparing the P-L relations in apparent magnitudes with equations (6) and (7) leads then to (provisional) apparent moduli μ_V and μ_I and their errors as shown in Figure 10 and repeated in Table 3.

Freedman et al. (2001) have suggested, based on LMC Cepheids given by Udalski et al. (1999b), that the P-L relation in I as given in equation (7) is too steep and that, consequently, all Cepheid distances should be reduced by ~7%. However, the situation is more complex.

Based on excellent photometry (Berdnikov, Voziakova, & Ibragimov 1995) and reddening values (Fernie et al. 1995)[4] of many hundreds of fundamental-mode Galactic Cepheids and on corresponding data of even more LMC Cepheids (Udalski et al. 1999a), Tammann et al. (2003b) have shown that the period-color relations of these two galaxies are distinctly different and that therefore also their P-L relations must differ for different wavebands. The new, quite steep Galactic P-L relations are calibrated

[4] See http://ddo.astro.utoronto.ca/cepheids.html.

TABLE 3
INDIVIDUAL DISTANCE MODULI AND REDDENING VALUES OF CEPHEIDS IN M83

	MF P-L[a]				GALACTIC P-L[b]				LMC P-L[c]			
ID	μ_V	μ_I	E[d]	μ_0	μ_V	μ_I	E[d]	μ_0	μ_V	μ_I	E[d]	μ_0
C1	28.15	27.94	0.21	27.64	28.20	28.03	0.17	27.78	28.05	27.83	0.22	27.52
C2	28.81	28.72	0.09	28.60	28.90	28.84	0.06	28.76	28.68	28.58	0.10	28.45
C3	28.95	29.03	−0.08	29.15	28.94	29.06	−0.12	29.23	28.90	28.96	−0.06	29.05
C4	28.62	28.49	0.13	28.31	28.62	28.54	0.08	28.41	28.54	28.41	0.13	28.21
C5	28.76	28.56	0.20	28.28	28.74	28.58	0.16	28.36	28.70	28.49	0.21	28.19
C6	29.45	28.84	0.61	27.95	29.43	28.86	0.57	28.04	29.39	28.77	0.62	27.86
C7	28.79	28.71	0.08	28.58	28.80	28.75	0.05	28.68	28.72	28.62	0.10	28.48
C8	28.54	28.50	0.04	28.45	28.40	28.42	−0.02	28.44	28.57	28.50	0.07	28.42
C9	28.47	28.13	0.34	27.64	28.32	28.03	0.29	27.61	28.52	28.15	0.37	27.62
C10	28.69	28.39	0.30	27.95	28.56	28.30	0.26	27.94	28.72	28.39	0.33	27.91
C11	28.74	...	...	...	28.70	...	...	...	28.69	...	...	...
C12	29.29	...	...	...	29.20	...	...	...	29.28	...	...	...
Mean	28.72	28.53	0.19	28.26	28.69	28.54	0.15	28.33	28.68	28.47	0.21	28.17
	±0.11	±0.10	0.06	±0.15	±0.11	±0.11	0.06	±0.16	±0.11	±0.10	0.06	±0.15

[a] P-L relation of Madore & Freedman 1991.
[b] Galactic P-L relation (eqs. [8] and [9]).
[c] LMC P-L relation (eqs. [10] and [11]).
[d] $E = E(V-I) = \mu_V - \mu_I$.

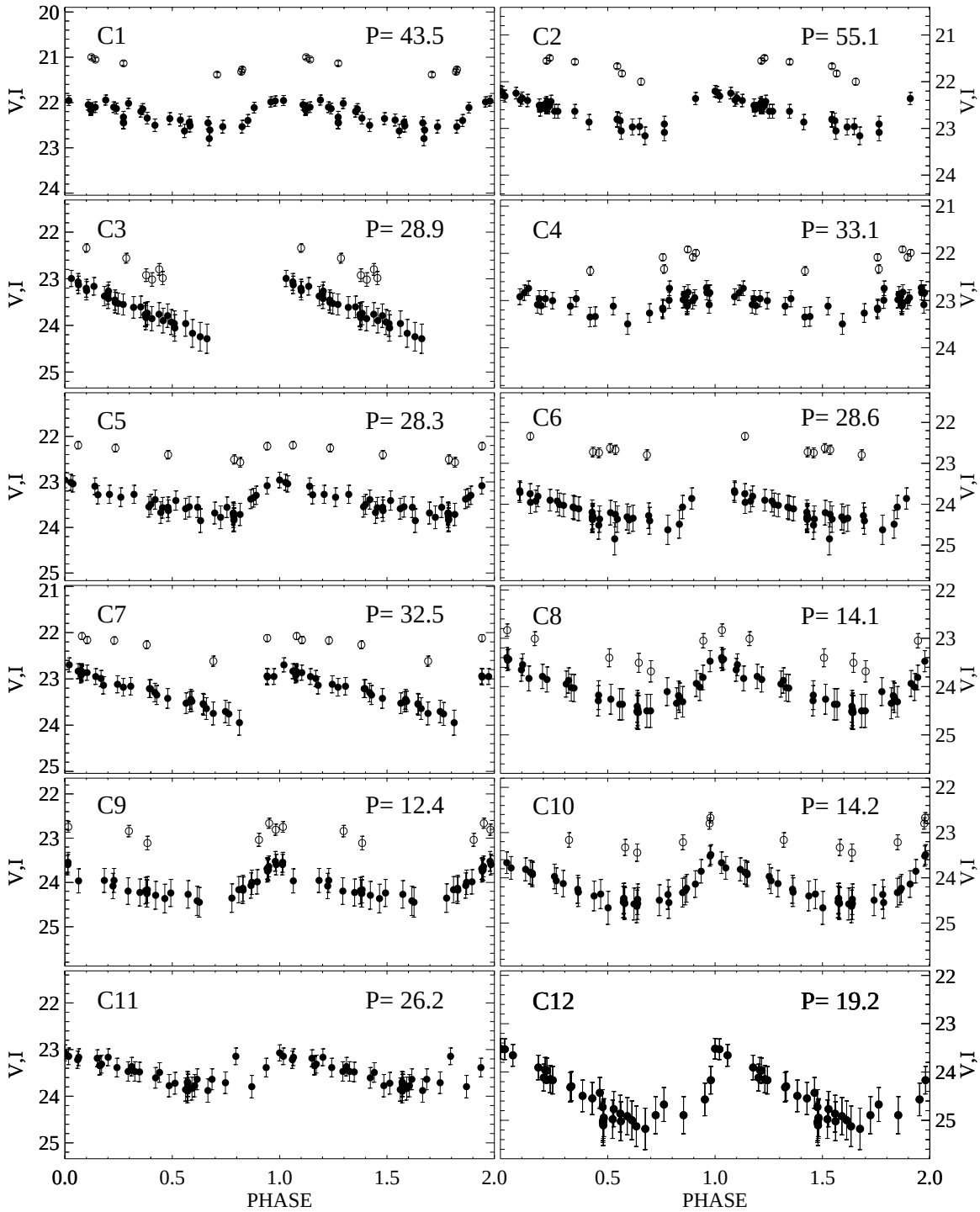

FIG. 9.—Light curves of 10 Cepheids in V (*filled circles*) and I (*open circles*). Two additional Cepheids, C11 and C12, have no measurements in I.

by 25 fundamental pulsators in open clusters and associations (Feast 1999; based on a Pleiades zero point of $\mu_0 = 5.61$ [Stello & Nissen 2001]) *and* independently by 28 fundamental pulsators whose purely physical distances have been derived by Gieren, Fouqué, & Gómez (1998) from the Baade-Becker-Wesselink method as revised by Barnes & Evans (1976). The adopted calibration agrees also with the *Hipparcos* analysis by Groenewegen & Oudmaijer (2000) to within $\sim 0.20 \pm 0.15$ mag, the latter being brighter.

The new Galactic P-L relations are given by Tammann et al. (2003b):

$$M_V = -3.14 \log P - 0.83 , \quad (8)$$

$$M_I = -3.41 \log P - 1.33 . \quad (9)$$

Preliminary P-L relations of the LMC were derived from 650 dereddened fundamental pulsators with good photometry by Udalski et al. (1999a). Assuming again $(m - M)^0 = 18.50$, G. A. Tammann, A. Sandage, & B.

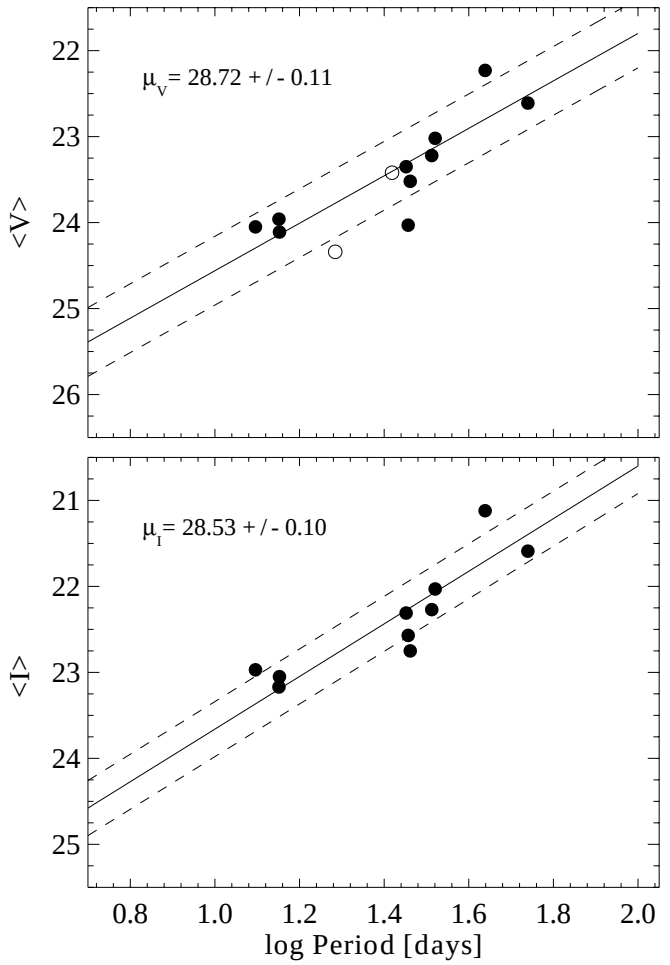

FIG. 10.—P-L relation of M83 in V (*top*) and I (*bottom*) for all 12 Cepheids in V and all 10 Cepheids in I. The solid lines represent the best fit with the canonical slope of -2.76 in V and -3.06 in I. The Cepheids C11 and C12 with no I magnitude are plotted with open circles. The dashed lines account for an adopted intrinsic width of the instability strip of ± 0.4 mag in V and ± 0.32 mag in I.

Reindl (2003, in preparation) and Tammann et al. (2003a) found for the LMC Cepheids with $\log P > 1.0$

$$M_V = -2.48 \log P - 1.75 , \tag{10}$$

$$M_I = -2.82 \log P - 2.09 . \tag{11}$$

There is no question that the slopes of the P-L relations in the Galaxy and in the LMC are *different*, the Galactic slope being steeper for long-period Cepheids.

4.2. *The Adopted Distance Modulus*

To determine a true distance modulus $(m - M)^0$ from the apparent Cepheid moduli in V and I, the ratio between $E(B-V)$ and the absorption in V and I is needed, i.e., A_V and A_I. We adopt the following values, which have been specifically derived for Cepheids (Tammann et al. 2003b):

$$R_V = \frac{A_V}{E(B-V)} = 3.17 , \tag{12}$$

$$R_I = \frac{A_I}{E(B-V)} = 1.87 . \tag{13}$$

The small color dependence of R can be neglected here because of the restricted range of Cepheid colors. The true distance modulus μ_0 becomes then

$$\mu_0 = 2.44\mu_I - 1.44\mu_V . \tag{14}$$

At this point it is not clear which of the three P-L relations discussed in § 4.1 should be applied to the M83 Cepheids: the P-L relations of Madore & Freedman (1991) as derived from the LMC data available at the time, the new P-L relations of the LMC (again at $\mu^0_{\rm LMC} = 18.50$), or the Galactic P-L relations whose slopes *and* zero point depend on purely Galactic data. Therefore, all three versions have been applied to the individual Cepheids of M83. The individual apparent moduli μ_V and μ_I are transformed into a true modulus μ_0 by means of equation (14). The results are shown in Table 3.

The three solutions in Table 3 differ by 0.16 mag at most. This near agreement is a fortuitous result and occurs because the Galactic and LMC P-L relations cross over not far from the median period (28.9 days) of the Cepheids under consideration.

If metallicity is the main reason for the different P-L relations in the Galaxy and in the LMC, then the distance modulus based on the Galactic P-L relation is more applicable, because M83 with [Fe/H] = 0.3 (Calzetti et al. 1999) is chemically more comparable with the Galaxy than with the metal-poor LMC. However, since we have at present no way of proving that metallicity only decides about the slope of the P-L relations, we adopt a mean modulus of

$$\mu_0 = 28.25 \pm 0.15 \text{ (statistical error)} \pm 0.15 \text{ (systematic error)} , \tag{15}$$

which corresponds to $4.5 \pm 0.3 \pm 0.3$ Mpc. The statistical error of 0.15 is the standard error of the different true distance moduli for each Cepheid in Table 3. The estimated systematic error is driven mainly by the difficult photometry and the nonuniqueness of the P-L relation of Cepheids.

Four of our Cepheids, C1, C3, C4, and C9, can be alleged to be less than fully convincing. By removing various combinations of these four Cepheids from the sample, we can change the distance modulus to vary between 28.16 and 28.42, which is consistent with our estimate.

4.3. *Comparison with Previously Published Distances*

The Cepheid distance of M83 is important in as much as the galaxy does not render easily to other methods of distance determination. An early distance of 8.9 Mpc, based on the size of the largest H II regions (Sandage & Tammann 1974), was much too large, presumably because its largest H II regions are relatively small, particularly for an Sc I–II galaxy, as it was classified at the time. De Vaucouleurs (1979) derived a distance of 3.7 Mpc from several of his distance indicators. Pierce's (1994) Tully-Fisher distance of 4.8 ± 1.0 Mpc is unreliable because M83 with an inclination of only 34° is not well suited for the method. Adopting a more recent luminosity class II for M83 and an apparent magnitude of $m^{0,i}_B = 8.08$ (corrected for Galactic and internal absorption; Sandage & Tammann 1987) and combining this with Sandage's (2000) calibration of Sc II galaxies of $M_B = -20.36 \pm 0.68$ ($H_0 = 50$) yields 4.9 ± 1.8 Mpc, which is even more insecure because of the wide luminosity scatter among Sc II galaxies. A model-dependent distance

comes from the expansion parallax of the SN II 1968L in M83 of 4.5 ± 0.8 (Schmidt et al. 1994). Of particular interest is the tip of the red giant branch (TRGB) distance of M83 by Karachentsev et al. (2002a), who found $\mu_0 = 28.27 \pm 0.15$.

5. COMPARISON OF THE DISTANCES OF NGC 5253 AND M83

A comparison of the distance of M83 to that of NGC 5253, which has produced the SNe Ia 1895B and 1972E, is interesting because it has been suggested that the two galaxies have interacted roughly 1 Gyr ago (van den Bergh 1980; Calzetti et al. 1999). In that case they are expected to be still rather close neighbors. This issue is made even more acute given the 0.4 mag difference between the distance of NGC 5253 by Gibson et al. (2000) and the original distance by the *HST* Supernovae Consortium (HSTSNC; Saha et al. 1995; Tammann et al. 2003a), even though they are both based on Cepheids.

The HSTSNC reduced their *HST* observations with two reduction packages: ROMAFOT as implemented in MIDAS was used at Basel by L. Labhardt and H. Schwengeler, and the modified DoPHOT reduction procedure as applied in Baltimore was used by A. Saha. The resulting magnitudes are in (very) good agreement, including the $\langle V \rangle$ and $\langle I \rangle$ magnitudes of the five Cepheids in common that were accepted by HSTSNC as being reliable.

The modulus of NGC 5253, corresponding to $\mu_0 = 28.08$, was determined by the HSTSNC from these five excellent Cepheids. The apparent modulus μ_V from the DoPHOT photometry of *seven additional* Cepheids is in agreement with that from the five "excellent" ones. However, in our judgment the I magnitudes for these seven are not as reliable: they fall below our adopted DoPHOT signal-to-noise ratio threshold for reliable detection.

One must also appreciate that the aberrated *HST* produced images at the time with diffraction structure that could easily result in *false detections*, for which reason the detection thresholds had to be kept high. To that was added the problem of the very crowded nature of these fields. There was therefore good reason to keep the selection criterion for acceptable Cepheids very conservative.

While a good many other putative variables were in fact detected both in Baltimore and at Basel, they were not considered further for fear of polluting with specious objects and erroneous photometry. If the errors in the apparent moduli in V and I for the five excellent Cepheids are propagated, the formal uncertainty is ± 0.28 mag. With this in mind, the path taken by the HSTSNC was to examine the *differential* extinction between Cepheids and the SN Ia 1972E in NGC 5253, which is shown to provide tighter constraints on the SN Ia calibration. This bypassed the difficulty of obtaining the distance *per se* to NGC 5253, when the real goal was to calibrate M_V for the SN Ia.

The *HST* observations were reanalyzed by Gibson et al. (2000), as part of their competing effort by the Mould-Freedman-Kennicutt (MFK) et al. group's work to obtain H_0. They used a different philosophy of adoption or rejection of candidates. In their re-reduction of the NGC 5253 data, Gibson et al. (2000) claimed to find several additional Cepheids not already published by Saha et al. (1995). These fainter additional objects would not have survived the more conservative selection criteria of Saha et al. (1995). They would have been deemed unusable. Of the seven Cepheids used by Gibson et al., only two are in common with the five excellent ones from Saha et al. (1995). In addition, three objects were found by both studies, *but were judged unusable* by Saha et al. (1995). The remaining two from Gibson et al. (2000) were not found in the Saha et al. study. The reported photometry from the five objects in common are in good agreement in both V and I (see Gibson et al. 2000, Table 3), even though three of them were not used by Saha et al. (1995). The comparison makes it clear *that it is not the photometry that is in question*, as also pointed out by Gibson et al. (2000), but that the distance derived is sensitive to the *sample* of Cepheids chosen.

We believe that the conservative selection of the five Cepheids in Saha et al. (1995) yields a more reliable sample compared to the seven Cepheids used by Gibson et al. (2000), particularly since three of the latter seven were explicitly rejected by Saha et al. (1995) and the remaining two were not found by them. In this context it is worth remarking that in obtaining distances to the galaxies observed by the MFK et al. project, only those Cepheids were used that were deemed worthy by both the ALLFRAME-based procedure and by the DoPHOT-based one. The DoPHOT procedure used by the MFK et al. group was identical to the one used by the HSTSNC. By this reckoning, only two Cepheids are in the common sample. Using averaged magnitudes from both studies for *only* these two common objects, we obtain $\mu_V = 28.08 \pm 0.18$, $\mu_I = 28.02 \pm 0.18$, and so $\mu_0 = 27.93 \pm 0.18$. This result is in better agreement with the Saha et al. (1995) value of 28.08 ± 0.28 than with the Gibson et al. (2000) result of $\mu_0 = 27.61 \pm 0.11$. In addition, the difficulties with other claims by Gibson et al. (2000), which we reject, concerning our previous photometry of other galaxies in the SN Ia calibration sample are discussed at length in Parodi et al. (2000).

In analogy to Table 3 we calculate the individual distances of the five accepted Cepheids of NGC 5253 in Table 4 using again the standard P-L relation of Madore & Freedman (1991) and the Galactic and LMC P-L relations by Tammann et al. (2003b) and G. A. Tammann et al. (2003, in preparation). Since NGC 5253 may be metal-poor, more comparable to the LMC than to the Galaxy, a Cepheid modulus of $\mu_0 = 28.09 \pm 0.25$ is adopted.

Another distance of NGC 5253 can be obtained from its SN Ia 1972E. The apparent magnitude at maximum for this SN is $m_V^{\rm corr}(\max) = 8.49 \pm 0.15$ (corrected for Galactic absorption, decline rate, and intrinsic color according to the prescription in Parodi et al. 2000); the internal absorption suffered by the SN Ia in its host galaxy is judged to be negligible on the basis of its outlying position and its color of $(B-V)_{\max} = -0.02$. This is bluer, if anything, than the mean reference color of $(B-V)_{\max} = -0.01$ of unreddened SNe Ia (see Parodi et al. 2000). The mean absolute magnitude of eight Cepheid-calibrated SNe Ia (excluding SN 1972E) is $M_V^{\rm corr} = -19.47 \pm 0.07$ (Saha et al. 2001b). From this follows a distance modulus of NGC 5253 of $\mu_0 = 27.96 \pm 0.19$, where the statistical error allows for the intrinsic scatter of ± 0.11 mag of the corrected absolute magnitude of SNe Ia (according to the same authors). The principal systematic error of this distance determination comes from the eight calibrating galaxies whose Cepheid distances are subject to the current problem of P-L relations not being the same in different galaxies.

TABLE 4
INDIVIDUAL DISTANCE MODULI OF CEPHEIDS IN NGC 5253

ID[d]	MF P-L[a]			GALACTIC P-L[b]			LMC P-L[c]		
	μ_V	μ_I	μ_0	μ_V	μ_I	μ_0	μ_V	μ_I	μ_0
C2-V3	28.24	28.03	27.72	28.03	27.88	27.65	28.33	28.09	27.74
C3-V2	27.95	28.31	28.83	27.78	28.20	28.80	28.00	28.33	28.81
C3-V6	28.37	28.28	28.14	28.10	28.06	28.03	28.44	28.34	28.19
C4-V2	28.08	27.79	27.37	27.94	27.70	27.36	28.11	27.79	27.34
C4-V3	27.81	28.05	28.40	27.70	27.99	28.41	27.82	28.04	28.35
Mean	28.09	28.09	28.09	27.91	27.96	28.04	28.14	28.11	28.09
	±0.10	±0.09	±0.25	±0.07	±0.08	±0.26	±0.11	±0.10	±0.25

[a] P-L relation of Madore & Freedman 1991.
[b] Galactic P-L relation (eqs. [8] and [9]).
[c] LMC P-L relation (eqs. [10] and [11]).
[d] ID as in Saha et al. 1995.

The modulus of NGC 5253 from SN 1972E agrees well with that adopted from Table 4, which is based on the five Cepheids by Saha et al. (1995). Our conclusion is that the best weighted distance modulus is $\mu_0(\mathrm{NGC\ 5253}) = 28.01 \pm 0.15$ (4.0 ± 0.3 Mpc). It should be noted that if the distance of Gibson et al. (2000) had been used, SN 1972E would have become the faintest among nine Cepheid-calibrated SNe Ia and would be 2.5 σ below the mean absolute magnitude of the other eight SNe Ia (see Saha et al. 2001a).

The distance difference between M83 and NGC 5253 becomes then $\Delta\mu = 0.24 \pm 0.21$ (0.5 ± 0.4 Mpc), which is not inconsistent, given the errors, with zero. The projected distance is only 0.15 Mpc. An interaction of the two galaxies roughly 1 Gyr ago is therefore very possible.

The strongest suggestion for a gravitational interaction between M83 and NGC 5253 comes from the amorphous morphology of the latter. Hogg et al. (1998) found in an objective sample of 10 amorphous galaxies that all have a peculiar velocity field and that seven of them have nearby companions. One of the three sample galaxies to which they did not assign a companion is NGC 5253. The hypothesis of an interaction is supported by its very unusual gasdynamics (Kobulnicky & Skillman 1995) and by the upper age limit of 10^8–10^9 yr of the stellar population in the exceptionally large halo of NGC 5253 (van den Bergh 1980; Caldwell & Phillips 1989). Moreover, also M83 shows signs of a postinteraction; the complex dynamics in its unusually large, lopsided H I halo may otherwise be difficult to explain (Huchtmeier & Bohnenstengel 1981).

6. THE M83 GROUP

Karachentsev et al. (2002a) have divided the B6 (Cen A) group of Kraan-Korteweg & Tammann (1979) and Kraan-Korteweg (1986a, 1986b) into two subgroups: one centered on Cen A and the other on M83.

They list 28 certain or probable members of the Cen A group. For seven of them the authors have determined TRGB distances, their mean value being $\mu_0 = 27.80 \pm 0.04$ (3.63 ± 0.07 Mpc). For Cen A proper the authors give a TRGB distance of $\mu_0 = 27.81 \pm 0.15$, and Rejkuba (2002) $\mu_0 = 27.99 \pm 0.10$ from the TRGB and Mira stars. For 14 members of the Cen A group, Karachentsev et al. (2002a) also list v_{LG} velocities (their Table 2), corrected to the centroid of the Local Group and with a mean value of $v_{\mathrm{LG}} = 293 \pm 24$ km s^{-1} ($\sigma_v = 90$ km s^{-1}). The correction from heliocentric velocities $v_\odot$ to v_{LG} is large in the direction of Centaurus and sensitive to the adopted solar apex solution. The authors have adopted the solution of Karachentsev & Makarov (1996). We prefer the solution of Yahil, Tammann, & Sandage (1977), which has the advantage of being independent of any adopted distances and which excludes companion galaxies whose orbital motion may deteriorate the solution. In this case one obtains $\Delta v_{\mathrm{LG}} = -275$ (instead of -245) km s^{-1} and hence $v_{\mathrm{LG}} = 263 \pm 31$ km s^{-1} (allowing for an additional error of 20 km s^{-1} in Δv_{LG}) for the radial velocity of the Cen A group.

The M83 group with 11 members (including now NGC 5253) is clearly more distant. Karachentsev et al. (2002a) give TRGB distances for five dwarf members. Their mean distance is $\mu_0 = 28.57 \pm 0.15$. This compares reasonably with the adopted distances of M83 ($\mu_0 = 28.25 \pm 0.15$ from Cepheids) and NGC 5253 ($\mu_0 = 28.01 \pm 0.15$ from Cepheids and SN 1972E). Combining the distances of the dwarfs, M83, and NGC 5253 gives a mean distance of the M83 group of $\mu_0 = 28.28 \pm 0.10$ (4.5 ± 0.2 Mpc), farther than the Cen A group.

Redshifts of 10 members of the M83 group are listed in the NASA Extragalactic Database. Their mean recession velocity is $v_\odot = 494 \pm 37$ km s^{-1} or, with $\Delta v_{\mathrm{LG}} = -245 \pm 20$ km s^{-1} (Yahil et al. 1977), $v_{\mathrm{LG}} = 249 \pm 42$ km s^{-1}. The additional correction to this value for a Virgocentric infall model is very small because M83 lies close to the surface, where the velocity components (in the radial direction of the observer) of the respective Virgocentric velocity vectors of the Local Group and of M83 nearly cancel (see Kraan-Korteweg 1986a, 1986b). If the local infall vector is assumed to be 220 km s^{-1}, Δv_{220} becomes +3 km s^{-1} taking the M83 group at 4.5 Mpc and the Virgo Cluster at 21.5 Mpc. An observer at the centroid of the Local Group would therefore observe a recession velocity of the M83 group of 252 ± 42 km s^{-1} if there were no disturbance from the Virgo complex.

The distances of the Cen A and M83 groups as seen from the centroid of the Local Group, assumed to lie between the Galaxy and M31 at two-thirds of the M31 distance (Sandage 1986), are 0.5 Mpc larger than as seen from the Sun; hence, $r(\mathrm{LG - Cen\ A}) = 4.13 \pm 0.1$ Mpc and $r(\mathrm{LG - M83}) = 5.0 \pm 0.2$ Mpc. In the case of pure Hubble flow and a cosmic value of $H_0 = 60$ (Parodi et al. 2000; Saha

et al. 2001b; Tammann et al. 2003a), the predicted group velocities would be $v_{\rm LG}({\rm Cen\ A}) = 248 \pm 6$ and $v_{\rm LG}({\rm M83}) = 300 \pm 12$ km s^{-1}. These values differ from the observed ones by only -15 ± 32 and $+48 \pm 44$ km s^{-1}. Thus, the deviations from pure Hubble flow remain within the measurement errors.

7. CONCLUSIONS

Twelve Cepheids with periods of 12 days $< P <$ 55 days were found in NGC 5236 (M83) with the 8.2 m Antu (UT1) telescope of the VLT. This shows that the telescope in its present configuration can be used for work on Cepheids out to $\sim$5 Mpc. The advantage over the much used WFPC2 of *HST* is the wider field and the better sampling of stellar images. Disadvantages are the enhanced problem of crowding and the larger number of epochs required for period determinations, because an optimized epoch distribution is hampered by external observing conditions. In spite of this, the total exposure time needed for M83 (60,000 s) is somewhat shorter than for a typical Cepheid distance with the WFPC2 (85,000 s).

The photometry was carried out with ROMAFOT. One epoch in V and I was independently reduced with DoPHOT and HSTPHOT. The photometric zero points agree to within ± 0.03 mag at $V = 20.0$ and $I = 19.0$. The three magnitude systems show, however, a small difference in the photometric scales, leading to mean magnitude differences of $\lesssim 0.1$ mag at $I = 22.5$; the scale error at $V = 23.5$ is only about half this value. These differences are explained by the different philosophies of how to treat the galaxy background. This problem is inherent to all photometries of faint stars that are seen against a bright background.

The distance of M83 was derived from the 10 Cepheids that have good light curves in V and I using three different P-L relations, i.e., the steep Galactic P-L relation, calibrated through Cepheids in open clusters *and* with Baade-Becker-Wesselink distances, and two versions of the LMC P-L relation, both based on an assumed modulus of $(m - M)^0_{\rm LMC} = 18.50$. The resulting mean distance of M83 is found to be $(m - M)^0 = 28.25 \pm 0.15$ (4.5 ± 0.3 Mpc).

The distance of NGC 5253, based on its Cepheids and SNIa 1972E, is rediscussed. The resulting modulus of $(m - M)^0 = 28.01 \pm 0.15$ (4.0 ± 0.3 Mpc) confirms the earlier Cepheid distance by Saha et al. (1995) and disagrees with that of Gibson et al. (2000).

The hardly significant difference in radial distance between M83 and NGC 5253 and the small *projected* distance (0.15 Mpc) make it possible that the two galaxies have interacted in the past, which may be the origin of the unusual amorphous type of NGC 5253.

The importance of the distances of M83 and NGC 5253, strengthening the mean distance of the M83 group of $(m - M)^0 = 28.28 \pm 0.10$ based also on TRGB distances of the dwarf members of Karachentsev et al. (2002a), is the continuing proof of the quietness of the local Hubble flow just outside the Local Group. Although the group is not the closest of the very local galaxies to the zero-velocity surface that separates the beginning of the expansion field from the bound galaxies of the Local Group (Sandage 1986), it nevertheless is close enough to be important for the eventual mapping of the position of this surface at the Local Group boundary.

At the time of Sandage (1986), the Im dwarf galaxies Leo A and Pegasus Dw (DDO 216) were considered to be well beyond the Local Group. Their low velocities reduced to the Local Group centroid are -32 and $+62$ km s^{-1}, respectively. These are very low for their large distances of 1.6 and 2.5 Mpc, assumed on the basis of the extant literature of 1986. It was this circumstance that gave considerable weight to the apparent detection of a deceleration due to the Local Group. Aparicio (1994) for Pegasus and Tolstoy et al. (1998) and Dolphin et al. (2002) for Leo A have shown that they are actually members of the Local Group. Aparicio (1994) and Dolphin et al. (2002) both derived a distance modulus of about $(m - M)^0 = 24.5$, whereas Tolstoy et al. (1998) derived $(m - M)^0 = 24.2$. *Hence, the evidence of deceleration based on Leo A and Pegasus has disappeared.*

The question of deceleration will be discussed in a forthcoming paper using galaxies near the edge of the Local Group such as Sextans A and B, the Antlia dwarf (LGS 3), GR 8, and NGC 300, as well as the M81/NGC 2403 and the IC 342 groups. *The emerging picture is that the expansion is already well in progress at a distance of* $\sim$1.5 Mpc (see Ekholm et al. 2001; Karachentsev et al. 2002b). The M83 group at 4.5 Mpc and with a corrected velocity of $v_{\rm LG} = 249$ km s^{-1} fits well into this picture.

The *absence* now of detectable deceleration of the velocity field outside the Local Group in the presence of a Local Group mass of $2 \times 10^{12}\ M_\odot$ (Sandage 1986; van den Bergh 1999; Evans et al. 2000) or even $4.9 \times 10^{12}\ M_\odot$, as suggested by its dynamical history (Lynden-Bell 1999), demands an explanation, as does the obviously *small dispersion* of the random velocities of the very local galaxies. This *coldness* of the velocity field in the presence of the clearly lumpy distribution of the visible matter has been a puzzle since 1972 (Sandage et al. 1972).

A modern suggestion that the total force field is nearly homogeneous (smooth) because of the dominance everywhere of an all-pervasive cosmological constant, diluting any lumpy gravity field of the clustered matter, has been put forward now by many, perhaps the first being Chernin, Teerikorpi, & Baryshev (2002). These considerations make a continual precision mapping of the local velocity field on a scale of 10 Mpc even more crucial. The work on M83 here is a contribution to this central problem.

We thank the VLT team, who performed so successfully the service-mode observations. F. T. and G. A. T. thank the Swiss National Science Foundation and the Swiss PRODEX program for financial support. F. T. thanks the National Optical Astronomy Observatory for its hospitality.

REFERENCES

Aparicio, A. 1994, ApJ, 437, L27
Barnes, T. G., & Evans, D. S. 1976, MNRAS, 174, 489
Berdnikov, L. N., Voziakova, O. V., & Ibragimov, M. A. 1995, Inf. Bull. Variable Stars, 4141, 1
Bertschinger, E. 1998, ARA&A, 36, 599
Buonanno, R., Buscema, G., Corsi, C. E., Ferraro, I., & Iannicola, G. 1983, A&A, 126, 278
Caldwell, N., & Phillips, M. M. 1989, ApJ, 338, 789
Calzetti, D., Conselice, C. J., Gallagher, J. S., & Kinney, A. L. 1999, AJ, 118, 797
Chernin, A., Teerikorpi, P., & Baryshev, Yu. 2002, Adv. Space Res., 31, 459
Davis, M., Efstathiou, G., Frenk, C. S., & White, S. D. M. 1985, ApJ, 292, 371

Davis, M., & Peebles, P. J. E. 1983, ApJ, 267, 465
de Vaucouleurs, G. 1979, AJ, 84, 1270
Dolphin, A. E., et al. 2002, AJ, 123, 3154
Ekholm, T. B., Baryshev, Yu., Teerikorpi, P., Hanski, M. O., & Paturel, G. 2001, A&A, 368, L17
ESO Image Processing Group. 1992, MIDAS User's Guide (Garching: ESO)
Evans, N. W., Wilkinson, M. I., Guhathakurta, P., Grebel, E. K., & Vogt, S. S. 2000, ApJ, 540, L9
Feast, M. 1999, PASP, 111, 775
Federspiel, M., Tammann, G. A., & Sandage, A. 1998, ApJ, 495, 115
Fernie, J. D., Evans, N. R., Beattie, B., & Seager, S. 1995, Inf. Bull. Variable Stars, 4148, 1
Freedman, W. L., et al. 2001, ApJ, 553, 47
Gibson, B. K. 2000, Mem. Soc. Astron. Italiana, 71, 693
Gibson, B. K., et al. 2000, ApJ, 529, 723
Gieren, W. P., Fouqué, P., & Gómez, M. 1998, ApJ, 496, 17
Governato, F., Moore, B., Cen, R., Stadel, J., Lake, G., & Quinn, T. 1997, NewA, 2, 91
Groenewegen, M. A. T., & Oudmaijer, R. D. 2000, A&A, 356, 849
Hogg, D. E., Roberts, M. S., Schulman, E., & Knezek, P. M. 1998, AJ, 115, 502
Hubble, E., & Humason, M. L. 1931, ApJ, 74, 43
———. 1934, Proc. Natl. Acad. Sci., 20, 264
Huchtmeier, W. K., & Bohnenstengel, H. D. 1981, A&A, 100, 72
Karachentsev, I. D., & Makarov, D. A. 1996, AJ, 111, 794
Karachentsev, I. D., et al. 2002a, A&A, 385, 21
———. 2002b, A&A, 389, 812
———. 2003, A&A, 398, 479
Kobulnicky, H. A., & Skillman, E. D. 1995, ApJ, 454, L121
Kraan-Korteweg, R. C. 1986a, A&AS, 66, 255
———. 1986b, A Catalog of 2810 Nearby Galaxies: The Effect of the Virgocentric Flow Model on Their Observed Velocities (Basel Preprint No. 18; Univ. Basel)
Kraan-Korteweg, R. C., & Tammann, G. A. 1979, Astron. Nachr., 300, 181
Krienke, O. K., & Hodge, P. W. 1974, AJ, 79, 1242
Labhardt, L., Sandage, A., & Tammann, G. A. 1997, A&A, 322, 751
Lafler, J., & Kinman, T. D. 1965, ApJS, 11, 216
Lynden-Bell, D. 1999, in IAU Symp. 192, The Stellar Content of the Local Group Galaxies, ed. P. Whitelock & R. Cannon (San Francisco: ASP), 39
Madore, B. F., & Freedman, W. L. 1991, PASP, 103, 933
Mateo, M. L. 1998, ARA&A, 36, 435
Ostriker, J. P. 1993, ARA&A, 31, 689
Parodi, B. R., Saha, A., Sandage, A., & Tammann, G. A. 2000, ApJ, 540, 634
Pierce, M. 1994, ApJ, 430, 53
Rejkuba, M. 2002, Ph.D. thesis, Univ. Católica Chile
Saha, A., Claver, J., & Hoessel, J. G. 2002, AJ, 124, 839
Saha, A., & Hoessel, J. G. 1990, AJ, 99, 97
Saha, A., Sandage, A., Labhardt, L., Schwengeler, H., Tammann, G. A., Panagia, N., & Macchetto, F. D. 1995, ApJ, 438, 8
Saha, A., Sandage, A., Tammann, G. A., Dolphin, A. E., Christensen, J., Panagia, N., & Macchetto, F. D. 2001a, ApJ, 562, 314
Saha, A., Sandage, A., Thim, F., Labhardt, L., Tammann, G. A., Christensen, J., Panagia, N., & Macchetto, F. D. 2001b, ApJ, 551, 973
Sandage, A. 1975, ApJ, 202, 563
———. 1986, ApJ, 307, 1
———. 2000, PASP, 112, 504
Sandage, A., & Brucato, R. 1979, AJ, 84, 472
Sandage, A., & Tammann, G. A. 1974, ApJ, 194, 559
———. 1975, ApJ, 196, 313
———. 1987, A Revised Shapley-Ames Catalog of Bright Galaxies (Publ. 635; Washington, DC: Carnegie Inst.)
Sandage, A., Tammann, G. A., & Hardy, E. 1972, ApJ, 172, 253
Schechter, P. L., Mateo, M. L., & Saha, A. 1993, PASP, 105, 1342
Schmidt, B. P., Kirshner, R. P., Eastman, R. G., Phillips, M. M., Suntzeff, N. B., Hamuy, M., Maza, J., & Aviles, R. 1994, ApJ, 432, 42
Stello, D., & Nissen, P. E. 2001, A&A, 374, 105
Szeifert, T., & Böhnhard, H. 2001, FORS1+2 User's Manual, VLT Paranal Obs.
Tammann, G. A., & Kraan, R. 1978, in IAU Symp. 79, The Large Scale Structure of the Universe, ed. M. S. Longair & J. Einasto (Dordrecht: Reidel), 71
Tammann, G. A., Reindl, B., Thim, F., Saha, A., & Sandage, A. 2003a, in ASP Conf. Ser. 283, A New Era in Cosmology, ed. N. Metcalfe & T. Shanks (San Francisco: ASP), in press
Tammann, G. A., Sandage, A., & Reindl, B. 2003b, A&A, in press
Thim, F. 2000, in IAU Colloq. 176, Impact of Large-Scale Surveys on Pulsating Star Research, ed. L Szabados & D. W. Kurtz (ASP Conf. Ser. 203; San Francisco: ASP), 231
———. 2001, Ph.D. thesis, Univ. Basel
Tolstoy, E., et al. 1998, AJ, 116, 1244
Udalski, A., Soszyński, I., Szymański, M., Kubiak, M., Pietrzyński, G., Woźniak, P., & Żebruń, K. 1999a, Acta Astron., 49, 223
Udalski, A., Szymański, M., Kubiak, M., Pietrzyński, G., Soszyński, I., Woźniak, P., & Żebruń, K. 1999b, Acta Astron., 49, 201
van den Bergh, S. 1980, PASP, 92, 122
———. 1999, A&A Rev., 9, 273
Yahil, A., Tammann, G. A., & Sandage, A. 1977, ApJ, 217, 903